Supplemental Figures

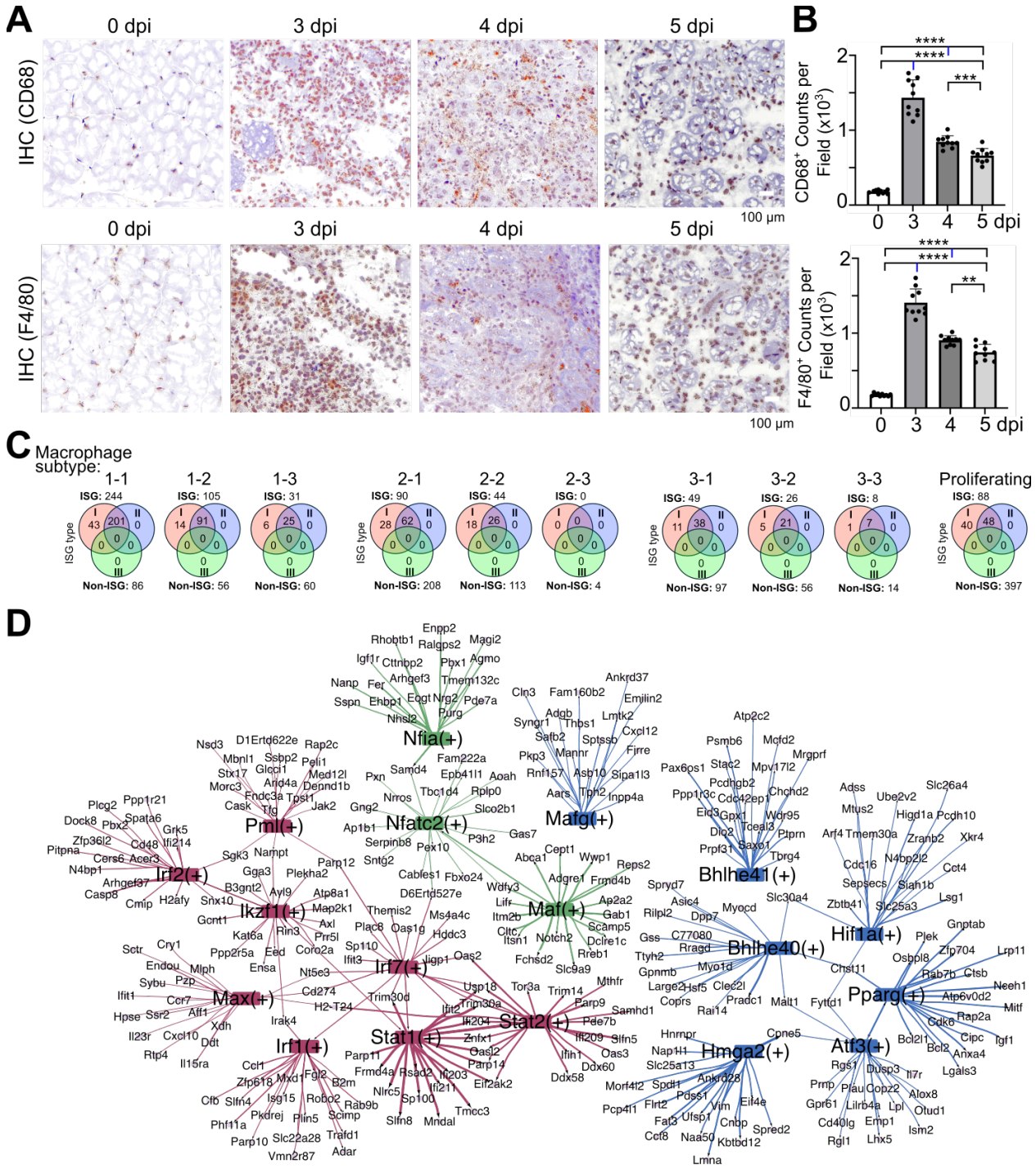

Fig. S1. Translational validation and interferon-associated regulatory programs of macrophage states during muscle regeneration. (A) Immunohistochemistry (IHC) staining of tibialis anterior (TA) muscle from uninjured, 3, 4, 5 days post-injury (dpi) following cardiotoxin (CTx) injection, stained for CD68 (upper) and F4/80 (lower). **(B)** Quantification of immune cell infiltration across regeneration time points based on histological

analyses. Data are shown as mean ± s.d.; n = 10 per group. Statistical significance was assessed using Mann-Whitney U (**P < 0.01, ***P < 0.001, ****P < 0.0001). **(C)** Proportions of interferon-stimulated genes (ISGs) among differentially expressed genes (DEGs) across macrophage subtypes, defined using Interferome database. **(D)** Gene regulatory network visualizations inferred by SCENIC, highlighting distinct transcription factor–centred regulon modules associated with inflammatory, reparative, and proliferative macrophage states. Nodes represent regulons and edges indicate regulatory associations, with colours denoting branch-specific enrichment.

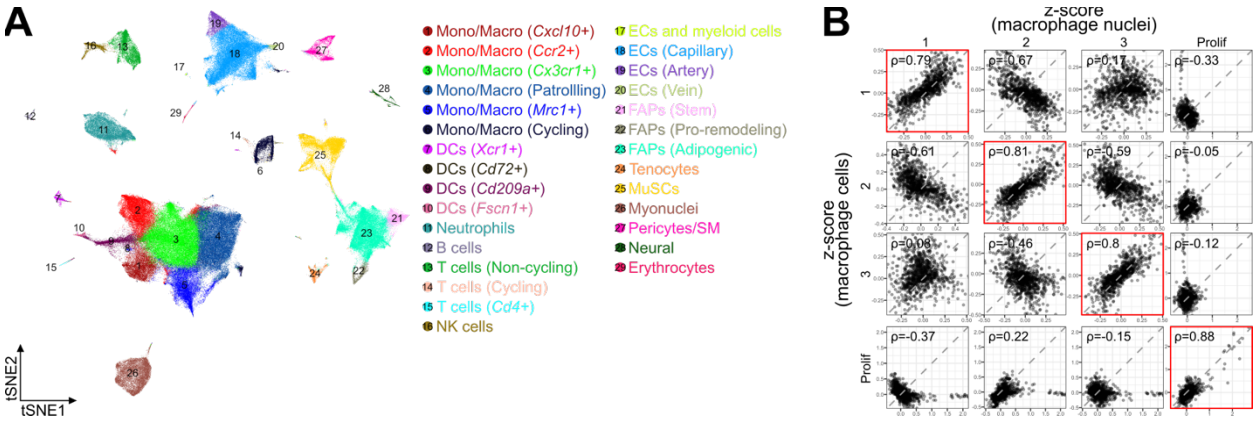

Fig. 2. Integration of snRNA- and scRNA-seq datasets resolves macrophage subpopulation identities. (A) Two-dimensional embedding of single cells (Walter *et al.* (*25*)). **(B)** Correlation analysis comparing macrophage transcriptional states defined by the snRNA-seq trajectory with corresponding populations from the scRNA-seq dataset (Walter *et al.* (*25*)). Scatter plots show average gene expression per state across modalities, with Pearson correlation coefficients indicated. Strong concordance is observed for the three main macrophage branches and the proliferative macrophage population.

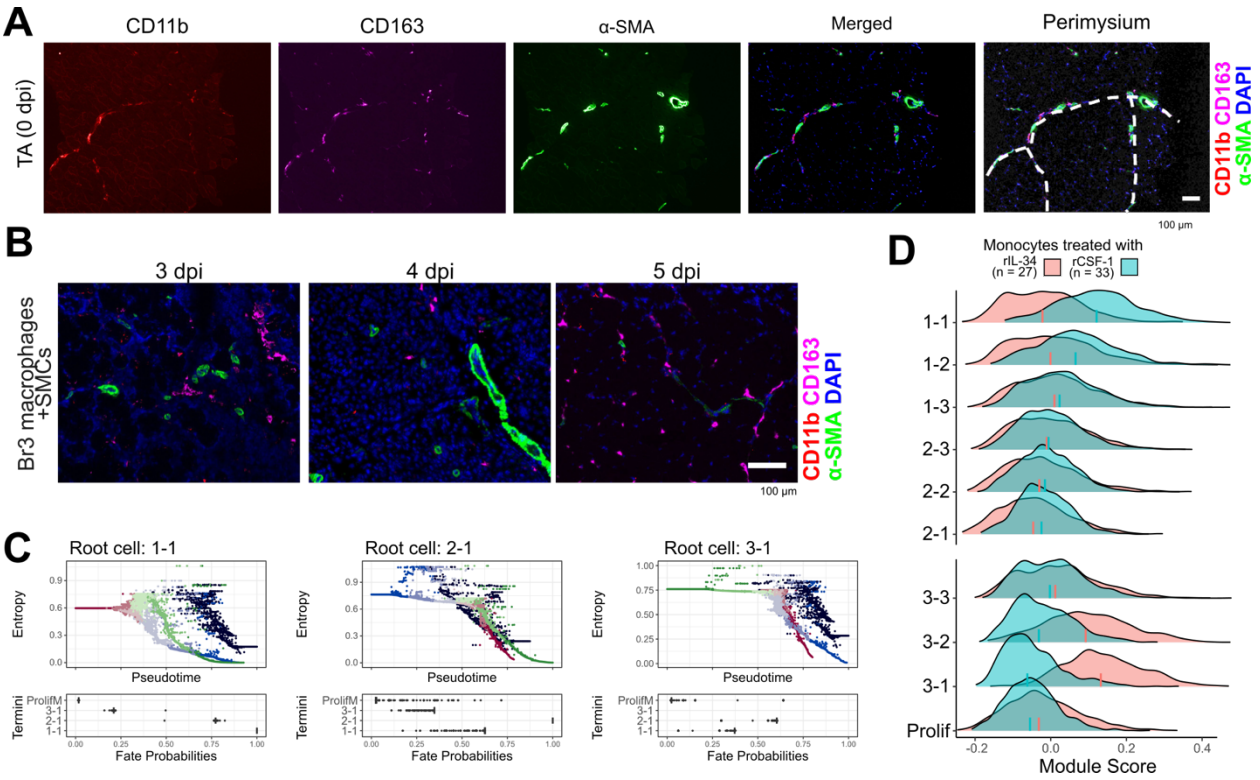

Fig. S3. Spatial segregation, niche association, and growth-factor responsiveness of macrophage subpopulations during muscle regeneration. **(A)** Representative immunofluorescence images of uninjured TA muscle (0 dpi) showing CD163$^+$ macrophages and their spatial association with α-SMA$^+$ mural cells within perimysial regions. Nuclei are counterstained with DAPI. **(B)** Immunofluorescence analysis of CD163$^+$ macrophages during regeneration showing redistribution from perimysial regions and reduced association with α-SMA$^+$ mural cells at 3–5 dpi. **(C)** Palantir fate-probability analysis. **(D)** Comparison of IL-34– and CSF-1–stimulated macrophage transcriptional signatures with branch-specific gene expression profiles.

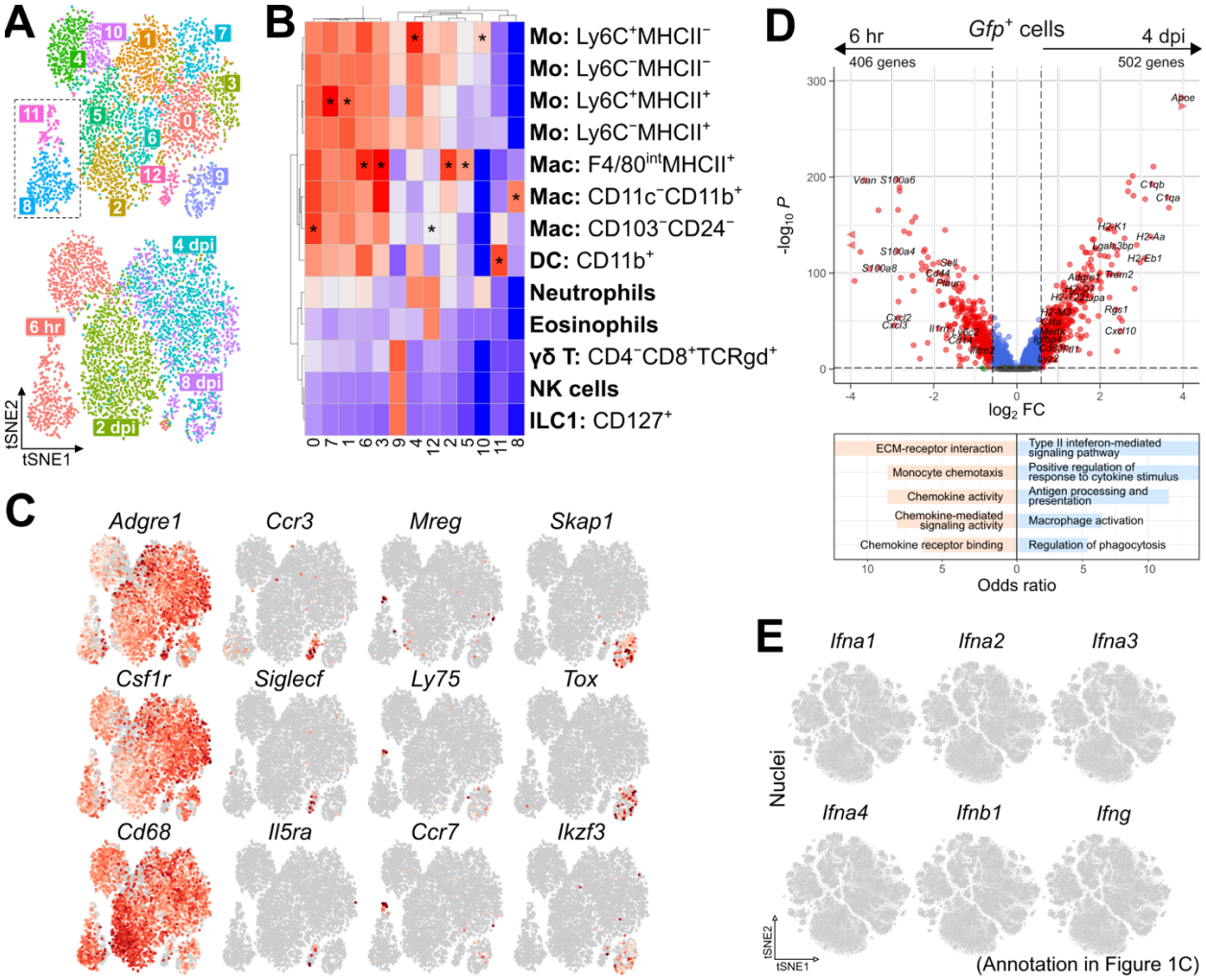

Fig. S4. Temporal transcriptional remodeling of monocyte-derived macrophages during muscle regeneration. **(A)** Two-dimensional embedding of the temporal scRNA-seq dataset incorporating parabiosis-based fate tracing, colored by transcriptional clusters (upper) and annotated by injury time points (lower). Spiked-in cells are encircled. **(B)** Annotation of immune clusters by reference mapping to ImmGen database. **(C)** Feature plots showing macrophage and other immune cell subclusters. **(D)** Differential gene expression and gene ontology (GO) enrichment analysis of genes upregulated in *Gfp*$^{+}$ cells at 6 h and 2 dpi stages. **(E)** Single-nucleus feature plots showing expression of type I and II interferon ligands across cell types within injured muscle.

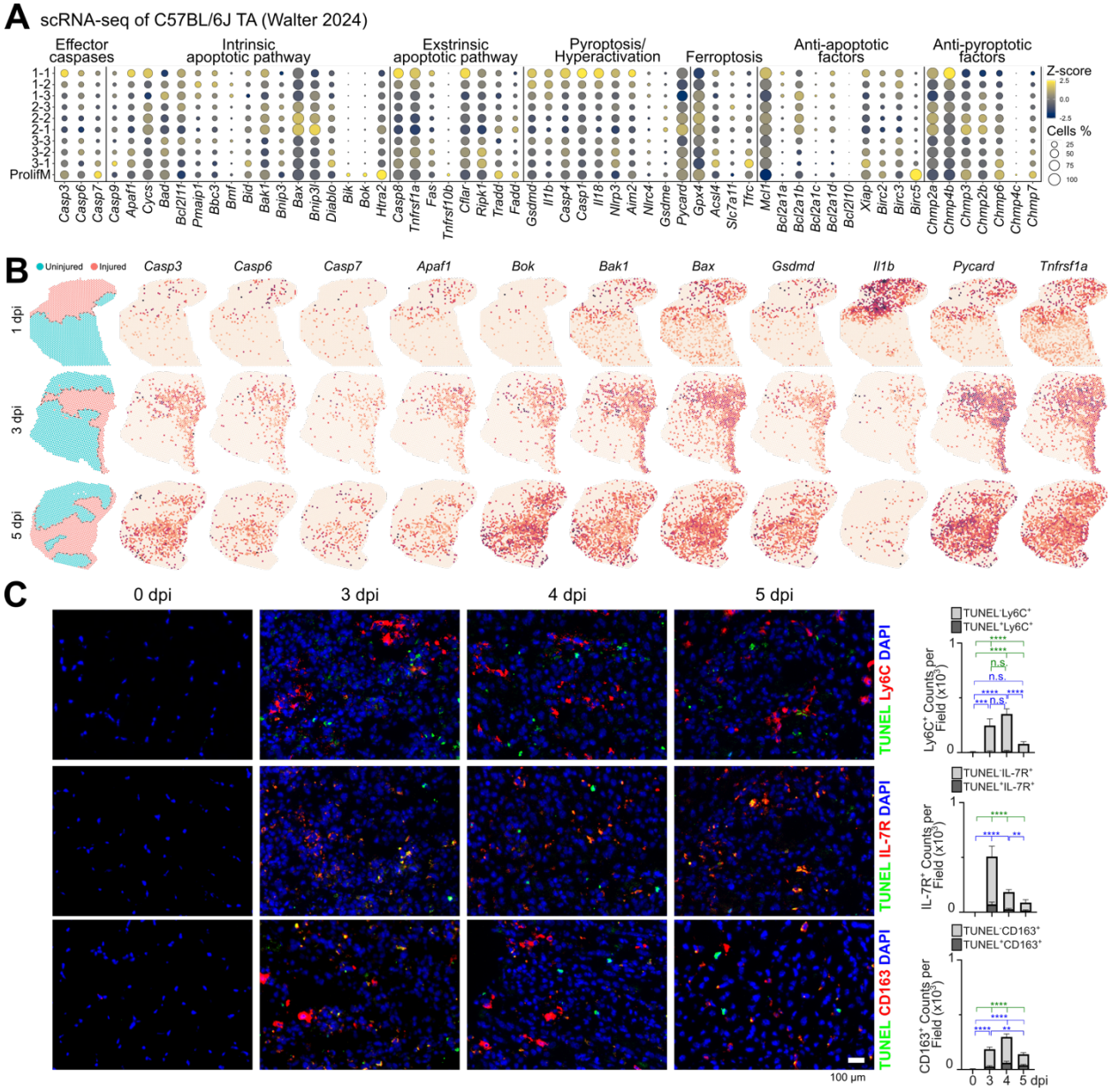

Fig. S5. Distinct cell death programs underlie the resolution of macrophage subpopulations during muscle regeneration. **(A)** Dot plot showing expression of genes associated with regulated cell death pathways across macrophage branches. **(B)** Spatial distribution of macrophage branches overlaid with expression of representative pyroptotic and apoptotic gene signatures, highlighting branch-specific enrichment patterns within injured muscle tissue. **(C)** Representative immunofluorescence images of injured TA muscle showing TUNEL staining combined with markers of macrophage subtypes (Ly6C, IL-7R, or CD163, as indicated).

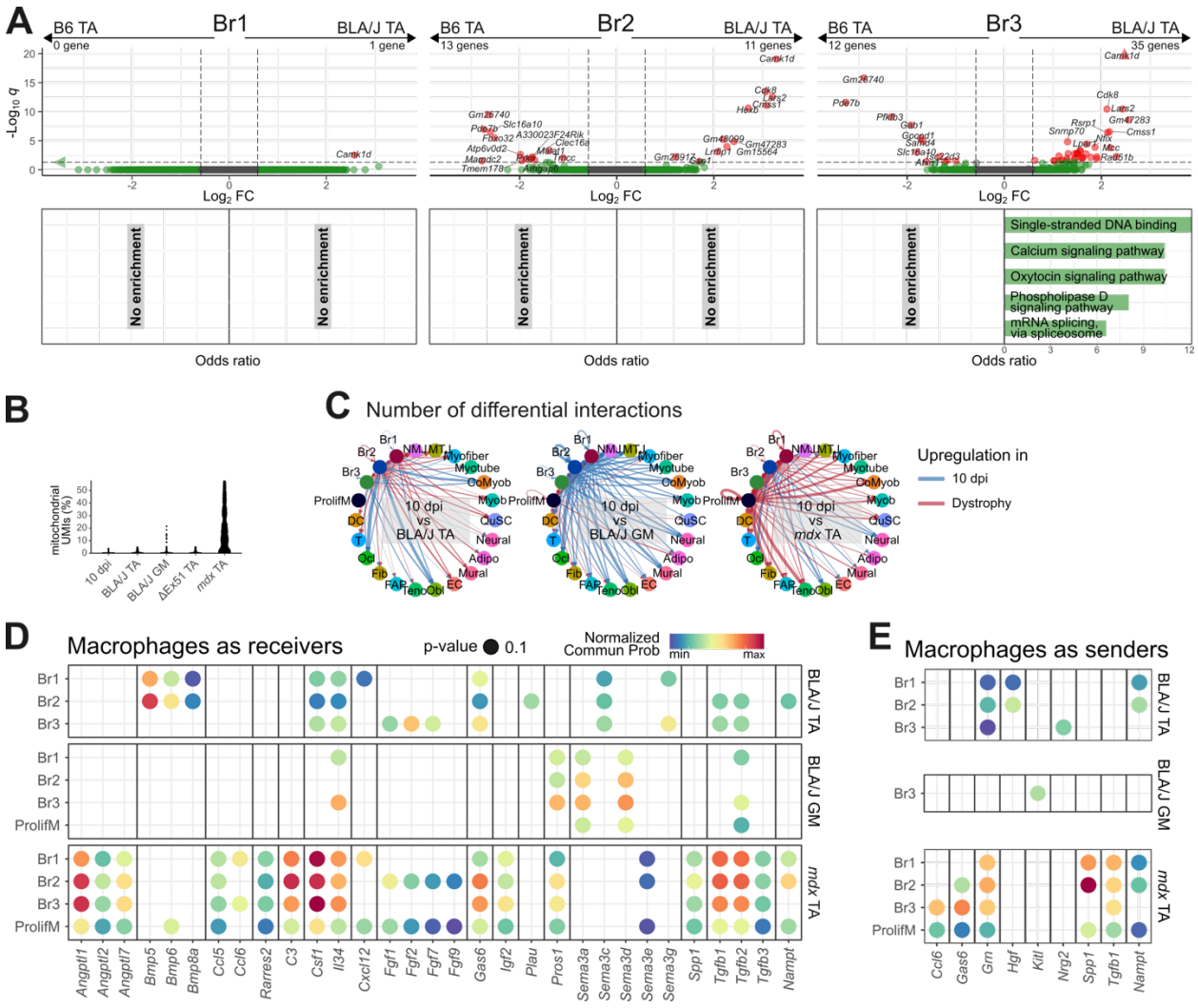

Figure S6. Macrophage-centred communication networks in dystrophic muscle. (A) snRNA-seq-based branch-specific differential gene expression and pathway enrichment analysis of macrophages from BLA/J GM projected onto the regenerative muscle-derived macrophage trajectory. **(B)** Quantitative comparison of data quality among analysed muscle samples. **(C)** CellChat-inferred ligand–receptor interaction analysis showing signals received by macrophages across branches. **(D)** Bidirectional CellChat analysis highlighting macrophage-derived signalling pathways.